Journal of Molecular Modeling (2019) 25: 33
https://doi.org/10.1007/s00894-018-3909-z

ORIGINAL PAPER

Diels-Alder reactivities of cycloalkenediones with tetrazine

Brian J. Levandowski[1] · Trevor A. Hamlin[2] · Hannah J. Eckvahl[1] · F. Matthias Bickelhaupt[2,3] · K. N. Houk[1]

Received: 22 September 2018 / Accepted: 17 December 2018 / Published online: 9 January 2019

Abstract

Quantum chemical calculations were used to investigate the Diels-Alder reactivities for a series of cycloalkenediones with tetrazine. We find that the reactivity trend of cycloalkenediones toward tetrazine is opposite to cycloalkenes. The electrostatic interactions between the cycloalkenediones and tetrazine become more stabilizing as the ring size of the cycloalkenediones increases, resulting in lower activation energies. The origin of the more favorable electrostatic interactions and the accelerated reactivities of larger cycloalkenediones result from a stabilizing CH/π interaction that is not present in the reaction of the 4-membered cycloalkenedione. The Diels-Alder reactivity trend of cycloalkenediones toward tetrazine is opposite that of cycloalkenes. The increased reactivity of the 5- and 6-membered cycloalkenediones relative to the 4-membered cycloalkenedione is attributed to a stabilizing electrostatic CH/π interaction that is not present in the reaction of the 4-membered cycloalkenedione.

Keywords Diels-Alder reaction · Distortion/interaction-activation strain model · Reactivity · Electrostatic interactions · Density functional theory

Introduction

The relationship between strain and reactivity in Diels-Alder reactions of cyclic dienophiles has been the subject of a number of experimental and theoretical studies. Scheme 1 shows the unusually high reactivity of cyclobutenone relative to cyclopentenone and cyclohexenone in the Diels-Alder reaction with cyclopentadiene [1]. The enhanced dienophilicity of cyclobutenone relative to larger cycloalkenones is generally attributed to strain release [2, 3]. Paton et al. studied computationally the Diels-Alder reactivity of a series of strained cycloalkenones with cyclopentadiene and refuted the relationship between strain and reactivity by showing there is a poor correlation between the Diels-Alder activation energy and reaction energy (strain release) [1]. They related the trend in the reactivity to differences in the distortion energies of the strained cycloalkenones. Angle strain increases the s-character of the olefinic C–H bonds and decreases the energy required to distort the C–H bonds out of planarity. The same conclusion was later drawn by Liu et al. to describe the reactivity trend of the strained cycloalkenes experimentally observed by Sauer et al. in the inverse electron-demand Diels-Alder reaction with 3,6-bis(trifluoromethyl)tetrazine shown in Scheme 2 [4, 5].

We studied computationally the Diels-Alder reactivities of a strained cycloalkene series from cyclopropene to cyclohexene with 3,6-bis(trifluoromethyl)tetrazine and cyclopentadiene and explained the reactivity trend in terms of primary and secondary orbital interactions [6]. The strength of the secondary orbital interactions diminishes as the allylic π/CH_2 groups of the cycloalkene orient increasingly outward from cyclopropene to cyclohexene, decreasing the overlap of the secondary orbital interactions. When cyclopentadiene is the diene, the strength of the primary and secondary orbital

Dedication: Dedicated to Tim Clark, computational chemist and friend, on the occasion of his 70th birthday.

This paper belongs to the Topical Collection Tim Clark 70th Birthday Festschrift

Electronic supplementary material The online version of this article (https://doi.org/10.1007/s00894-018-3909-z) contains supplementary material, which is available to authorized users.

✉ F. Matthias Bickelhaupt
f.m.bickelhaupt@vu.nl

✉ K. N. Houk
houk@chem.ucla.edu

[1] Department of Chemistry and Biochemistry, University of California, Los Angeles 90095, CA, USA

[2] Department of Theoretical Chemistry and Amsterdam Center for Multiscale Modeling (ACMM), Vrije Universiteit Amsterdam, De Boelelaan 1083, 1081 HV Amsterdam, The Netherlands

[3] Institute for Molecules and Materials (IMM), Radboud University, Heyendaalseweg 135, 6525 AJ Nijmegen, The Netherlands

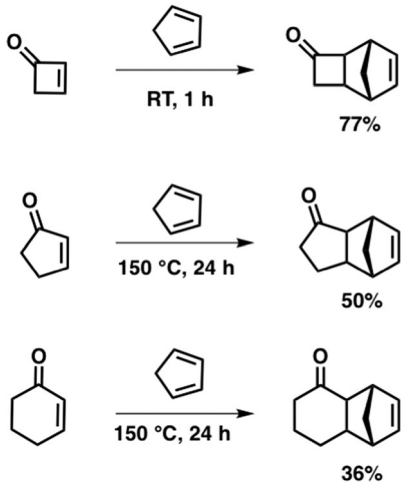

Scheme 1 Diels-Alder reactions of cyclopentadiene with cyclobutenone, cyclopentenone, and cyclohexanone [1]

interactions both increase from cyclohexene to cyclopropene, resulting in a 100 billion-fold difference in reactivity across the series. With 3,6-bis(trifluoromethyl)tetrazine, the increase in the strength of secondary orbital interactions from cyclohexene to cyclopropenes is counteracted, but not energetically overridden, by the primary orbital interactions, which weaken from cyclohexene to cyclopropene in the inverse electron-demand Diels-Alder reaction. This results in a smaller, 2 million-fold difference in reactivity across the cycloalkene series.

We have recently shown that the polarized nature of the carbonyl bond in cyclopropenones results in extremely weak secondary orbital interactions [7]. To determine how suppressing the strength of the secondary orbital interactions affects the reactivity trend of cyclic dienophiles, we investigated the Diels-Alder reactivity of the cycloalkenedione series **1**–**3** shown in Scheme 3 with the highly electron deficient 1,2,4,5-tetrazine (**Tz**).

Computational methods

We computed the activation free energies for the Diels-Alder reactions of **1**–**3** with **Tz** using the M06-2X [8] functional. Geometry optimizations were calculated in Gaussian 09 [9] at the M06-2X/6-31G(d) level of theory. Energies were

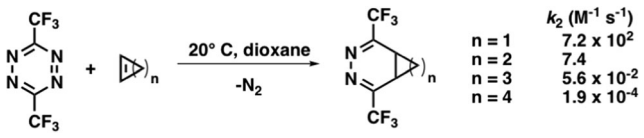

Scheme 2 Reactivities of strained cycloalkenes in the inverse electron-demand Diels–Alder reaction with 3,6-bis(trifluoromethyl)tetrazine [5]

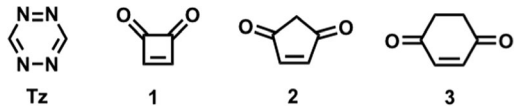

Scheme 3 Structures of Tz and the cycloalkenediones 1–3

obtained from single point calculations using the 6–311++ G(d,p) basis set. Insight into the factors governing the Diels-Alder reactivity of the cycloalkenediones with **Tz** was provided by the distortion/interaction-activation strain model [10]. The analysis decomposes the electronic energies ΔE into two terms: the distortion energy ΔE_{d} (also called activation strain) associated with deforming the individual reactants and the interaction ΔE_{int} between the deformed reactants. The ΔE_{int} term is then further assessed by an energy decomposition analysis (EDA), which decomposes the interaction energy term into three terms: (1) $\Delta V_{\mathrm{elstat}}$ corresponds to the electrostatic interactions; (2) $\Delta E_{\mathrm{Pauli}}$ is the closed shell repulsion energy (steric effects); and (3) ΔE_{oi} quantifies charge transfer, mainly between frontier molecular orbitals (FMO), as well as polarization. The distortion/interaction-activation strain and energy decomposition analysis were performed using the ADF.2017.103 program [11–13] at the M06-2X/TZ2P [8, 14, 15] level of theory on the M06-2X/6-31G(d) transition state geometries.

Results and discussion

The transition state structures and activation free energies ($\Delta G^{\ddagger}$) for the Diels-Alder reactions of **Tz** with **1**–**3** are shown in Fig. 1. The positions of the transition states occur at a similar point on the reaction coordinate, with forming bond lengths ranging from 2.12 to 2.14 Å. This can be attributed to the slight exergonicity of the reactions, which are similar and range from −1.4 to −3.0 kcal mol^{-1}. The Diels-Alder reactivities of **1**–**3** increase as the ring size of the cycloalkenediones increases. This is in contrast to the observed reactivity trends of cycloalkenes toward tetrazines, which decrease in reactivity as the ring size of the cycloalkenes increases [4–6]. The activation free energies for the Diels-Alder reactions of **2** and **3** with **Tz** are similar, with activation free energies of 26.1 and 25.5 kcal mol^{-1}, respectively, whereas the reaction of **1** with **Tz** is significantly less favorable, with an activation free energy of 29.7 kcal mol^{-1}. From the predicted relative reaction rates, **3** reacts 1200 times faster than **1** with **Tz**.

To understand the differences in the activation energies of **1**–**3** with **Tz**, we analyzed the transition states with the distortion/interaction-activation strain model [10]. Figure 2 shows the resulting distortion/interaction-activation strain analysis for the Diels-Alder reactions of **Tz** with **1**–**3**. The distortion energies are nearly identical for the

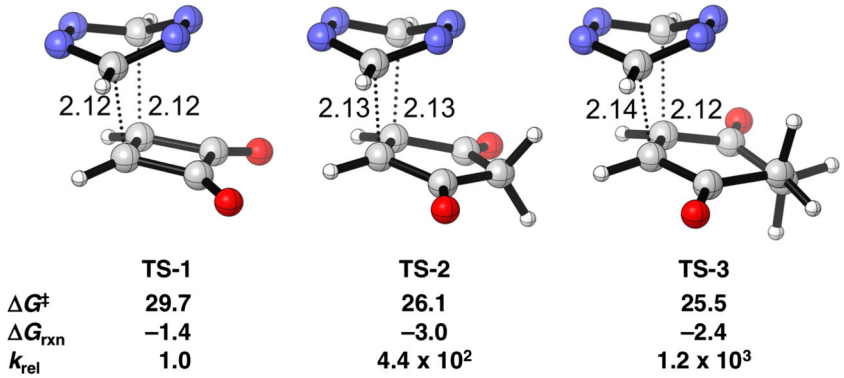

Fig. 1 Transition state structures with forming bond lengths in Å for the Diels-Alder reactions of **Tz** with **1**–**3**. The computed Gibbs activation free energies ($\Delta G^{\ddagger}$) and free energies of reaction (ΔG) are reported in kcal mol^{-1} at the M06-2X/6–311++G(d,p)//M06-2X/6-31G(d) level of theory. The predicted reaction rates (k_{rel}) relative to **1** are also provided.

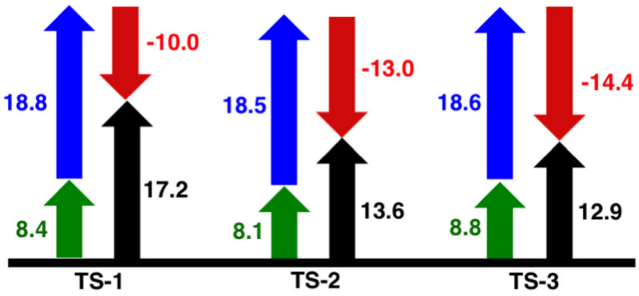

Fig. 2 Distortion/interaction-activation strain analyses (in kcal mol^{-1}) of **TS1**, **TS2**, and **TS3** computed at M06-2X/TZ2P//M06-2X/6-31G(d). Color code: (green, distortion energy of cycloalkenedienone; blue, distortion energy of **Tz**; red, interaction energy; black, activation energy)

cycloalkenediones and **Tz**, differing less than 1 kcal mol^{-1} across the series. The interaction energies, on the other hand, range from −10 to −14 kcal mol^{-1}. The difference in the reactivities of **1**–**3** is associated with differences in the interaction energies, which become more stabilizing as the ring size of the cycloalkenedione increases.

The results from the energy decomposition analysis (EDA) of the transition state interaction energies are summarized in Table 1. The ΔE_{oi} are similar for all reactions, ranging from only −62 to −63 kcal mol^{-1}. The ΔE_{Pauli}, which range from 100 to 104 kcal mol^{-1}, are most repulsive for **3** and weaken slightly as the ring size of the cycloalkenedione decreases. The ΔV_{elstat} at the transition states range from −47 to −55 kcal mol^{-1} and parallel the reactivity trend of the cycloalkenediones by becoming more stabilizing as the ring size of the cycloalkenedione increases. The EDA analysis reveals that the reactivity of the cycloalkenedione series is under electrostatic control.

The results of the frontier molecular orbital analysis are summarized in Table 2 and reveal that the reactions of **1**–**3** with **Tz** are neutral electron-demand cycloadditions. The frontier molecular orbital gaps for the normal and inverse electron-demand interactions of **1**–**3** with **Tz** are unfavorably large and range from 11.8 to 11.9 and 11.4 to 12.1 eV, respectively, with overlaps between 0.21 and 0.24. The cycloalkenediones and **Tz** are both highly electron-deficient substrates and there is little charge transfer between them at the transition state. The lack of charge transfer is consistent with a neutral electron-demand reaction.

The reactivity differences in the cycloalkene series shown in Scheme 2 with 3,6-bis(trifluoromethyl)tetrazine are controlled by secondary orbital interactions involving the overlap of the allylic π/CH_2 groups of the cycloalkene highest occupied molecular orbital (HOMO) with the lowest unoccupied molecular orbital (LUMO) of **Tz** [6]. The HOMOs of the cycloalkenediones are shown in Fig. 3. The polarized nature of the carbonyl reduces the HOMO coefficient at the carbon atoms of the carbonyl groups, and secondary orbital interactions between the HOMO of **1**–**3** and the LUMO of **Tz** are negligible due to the lack of appreciable electron density at the carbonyl carbons. The similarity of the frontier molecular

Table 1 Energy decomposition analysis (in kcal mol^{-1}) of the interaction energies performed on the transition state structures **TS1**, **TS2**, and **TS3** computed at M06-2X/TZ2P//M06-2X/6-31G(d)

System	ΔE_{int}	ΔE_{Pauli}	ΔV_{elstat}	ΔE_{oi}
TS1	−10.0	100.4	−47.1	−63.4
TS2	−13.0	101.0	−52.1	−61.9
TS3	−14.4	103.8	−55.4	−62.9

Table 2 Normal and inverse electron-demand frontier molecular orbital interactions for the reactions of **1**–**3** with **Tz**. FMO interactions and charge transfer calculated at HF/6–311++G(d,p)//M06-2X/6-31G(d) on transition state geometries of **1**–**3**. The FMO overlaps calculated at the HF/TZ2P//M06-2X/6-31G(d) level of theory are provided in parenthesis

Dione	Normal FMO gap (eV)	Inverse FMO gap (eV)	Charge transfer
1	11.9 (0.24)	12.1 (0.21)	0.02
2	11.8 (0.22)	11.6 (0.21)	0.00
3	11.8 (0.21)	11.4 (0.21)	0.00

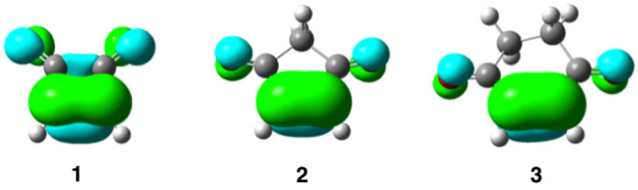

Fig. 3 Visualization (isovalue = 0.04) of the highest occupied molecular orbitals of **1**–**3**

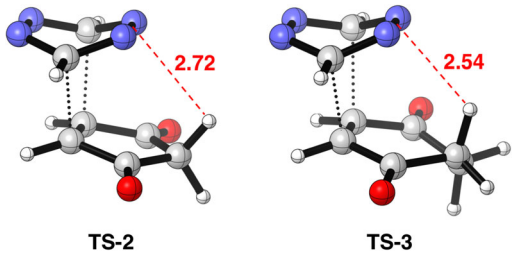

Fig. 5 Stabilizing CH/π interaction in the transition states of **2** and **3** with **Tz**. The distance between the hydrogen atom and the center of the forming π-bond is shown in Ångstroms

orbital shapes and energies is in good agreement with the orbital interactions (ΔE_{oi}) in Table 1, which are similar for the reactions of **1**–**3** with **Tz**.

To understand the trend in $\Delta V_{elstat}(\zeta)$, we analyzed the electrostatic potential maps (ESP) [16] and Hirshfeld charges for the transition state geometries of **Tz** and **1**–**3** (Fig. 4). Negative (red) ESP values from the potential maps indicate electron-rich regions, whereas positive (blue) regions represent electron-deficient regions [17]. The carbon atoms of **Tz** are relatively positive as a result of the electronegative nitrogen atoms, which pull electron density away from the carbon atoms and also reduces the aromaticity of the diene. The alkyl groups between the carbonyls of **2** and **3** create an electropositive (blue) region that interacts favorably with the electronegative (red) region surrounding the nitrogen atoms during the course of bond formation. Additionally, there is a stabilizing CH/π interaction in the transition states of **2** and **3** with **Tz** that is not present in the reaction of **1** with **Tz**. CH/π interactions are weak hydrogen bonds that have been found to play an important role in stereoselective organic reactions and biomolecule stability [18–21]. The CH/π interactions observed in **TS-2** and **TS-3** are shown in Fig. 5 and involve the partial positive charge of the hydrogen atom interacting with the negative region of the tetrazine scaffold. The distance between the hydrogen atom and the center of the forming π-bond is within the typical range for CH/π interactions at 2.72 and 2.54 Å for **TS-2** and **TS-3**, respectively [22].

Conclusions

We studied the Diels-Alder reactivities of a series of cycloalkenediones toward tetrazine with density functional theory. The predicted reactivity trend of the cycloalkenediones toward tetrazine is opposite to the reactivity trend observed in reactions of cycloalkenes toward tetrazine. An energy decomposition analysis concluded that the reactivity differences were related to the strength of the electrostatic interactions. The more favorable electrostatic interactions, and the accelerated reactivities of **2** and **3** relative to **1**, result from a stabilizing CH/π interaction present in the transition states of **2** and **3** with **Tz**, but not the reaction of **1** with **Tz.**

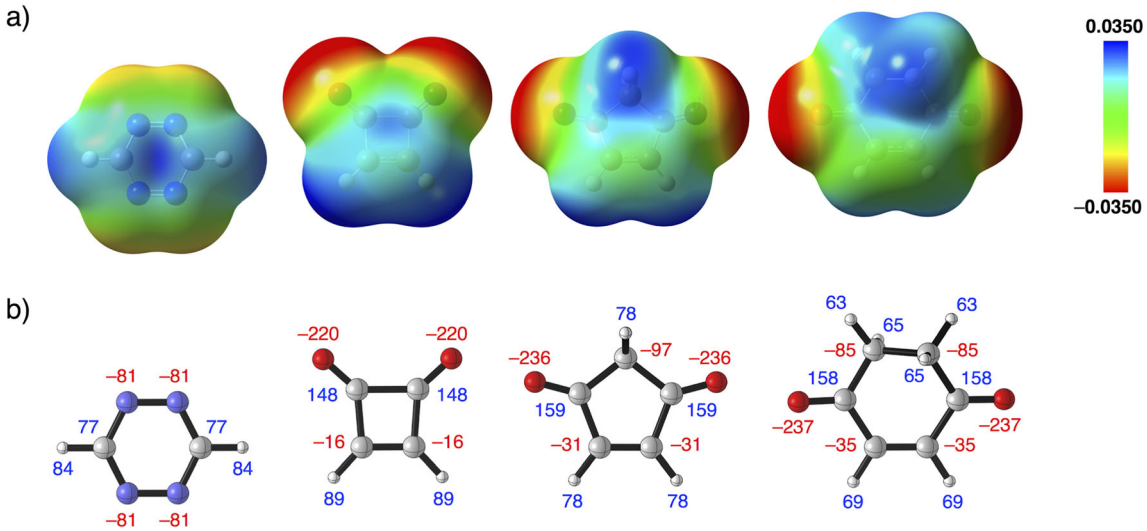

Fig. 4 (a) ESP maps (top row, left to right) of **Tz** and **1**–**3** from the transition state geometries using a consistent surface potential range of −0.0350 a.u. (red) to 0.0350 a.u. (blue) and an isovalue of 0.0004. The ESP maps were plotted on the total electron density from the M06-2X/6-31G(d) calculations. (b) Hirshfeld charges (m a.u.) (bottom row, left to right) of **Tz** and **1**–**3** computed at M06-2X/TZ2P//M06-2X/6-31G(d)

Acknowledgments We thank the National Science Foundation (NSF CHE-1361104), the National Institute of Health (NIH R01GM109078), and the Netherlands Organization for Scientific Research (NWO) for financial support. We thank Dennis Svatunek for helpful discussions and assistance in generating the ESP maps. Computer time was provided by the UCLA Institute for Digital Research and Education (IDRE) on the Hoffman2 supercomputer. We additionally thank SURFsara for use of the Cartesius supercomputer.

References

1. Paton RS, Kim S, Ross AG et al (2011) Experimental Diels-Alder reactivities of cycloalkenones and cyclic dienes explained through transition-state distortion energies. Angew Chem Int Ed 50:10366–10368
2. Belluš D, Ernst B (1988) Cyclobutanones and cyclobutenones in nature and in synthesis [new synthetic methods(71)]. Angew Chem Int Ed Engl 27:797–827
3. Li X, Danishefsky SJ (2010) Cyclobutenone as a highly reactive dienophile: expanding upon Diels-Alder paradigms. J Am Chem Soc 132:11004–11005
4. Liu F, Paton RS, Kim S et al (2013) Diels-Alder reactivities of strained and unstrained cycloalkenes with normal and inverse-electron-demand dienes: activation barriers and distortion/interaction analysis. J Am Chem Soc 135:15642–15649
5. Sauer J, Heldmann DK, Hetzenegger J et al (1998) 1,2,4,5-Tetrazine: synthesis and reactivity in [4 2] cycloadditions. Eur J Org Chem 2885–2896
6. Levandowski BJ, Hamlin TA, Bickelhaupt FM, Houk KN (2017) Role of orbital interactions and activation strain (distortion energies) on Reactivities in the normal and inverse electron-demand cycloadditions of strained and unstrained cycloalkenes. J Org Chem 82:8668–8675
7. Levandowski BJ, Hamlin TA, Helgeson RC et al (2018) Origins of the endo and exo selectivities in cyclopropenone, iminocyclopropene, and triafulvene Diels-Alder cycloadditions. J Org Chem 83:3164–3170
8. Zhao Y, Truhlar DG (2008) The M06 suite of density functionals for main group thermochemistry, thermochemical kinetics, noncovalent interactions, excited states, and transition elements: two new functionals and systematic testing of four M06-class functionals and 12 other functionals. Theor Chem Accounts 120:215–241
9. Frisch MJ, Trucks GW, Schlegel HB et al (2009) Gaussian 09, revision D.01. Gaussian, Inc., Wallingford
10. Bickelhaupt FM, Houk KN (2017) Analyzing reaction rates with the distortion/interaction-activation strain model. Angew Chem Int Ed 56:10070–10086
11. te Velde G, Bickelhaupt FM, Baerends EJ et al (2001) Chemistry with ADF. J Comput Chem 22:931–967
12. Fonseca Guerra C, Snijders JG, te Velde G, Baerends EJ (1998) Towards an order-N DFT method. Theor Chem Accounts 99:391–403
13. ADF (2017) SCM theoretical chemistry. Vrije Universiteit, Amsterdam. https://www.scm.com/
14. van Lenthe E, Baerends EJ (2003) Optimized Slater-type basis sets for the elements 1-118. J Comput Chem 24:1142–1156
15. Franchini M, Philipsen PHT, van Lenthe E, Visscher L (2014) Accurate coulomb potentials for periodic and molecular systems through density fitting. J Chem Theory Comput 10:1994–2004
16. Wheeler SE, Houk KN (2009) Through-space effects of Substituents dominate molecular electrostatic potentials of substituted Arenes. J. Chem. Theory Comput. 5:2301–2312
17. Politzer P, Truhlar DG (2013) Chemical applications of atomic and molecular electrostatic potentials: reactivity, structure, scattering, and energetics of organic, inorganic, and biological systems. Springer, New York
18. Hamlin TA, Hamann CS, Tantillo DJ (2015) Delocalization of charge and electron density in the humulyl cation—implications for terpene biosynthesis. J Org Chem 80:4046–4053
19. Levandowski BJ, Houk KN (2016) Hyperconjugative, secondary orbital, electrostatic, and steric effects on the reactivities and endo and exo stereoselectivities of cyclopropene Diels-Alder reactions. J Am Chem Soc 138:16731–16736
20. Nishio M, Umezawa Y, Honda K et al (2009) CH/π hydrogen bonds in organic and organometallic chemistry. CrystEngComm 11:1757
21. Nishio M, Umezawa Y, Fantini J et al (2014) CH–π hydrogen bonds in biological macromolecules. Phys Chem Chem Phys 16:12648–12683
22. Nishio M (2011) The CH/π hydrogen bond in chemistry. Conformation, supramolecules, optical resolution and interactions involving carbohydrates. Phys Chem Chem Phys 13:13873–13900